16th World Congress in Computational Mechanics (WCCM)
21-26 July 2024, Vancouver, Canada
A. Korobenko, M. Laforest, S. Prudhomme, R. Vaziri (Eds)

CREATING BIO-FIDELIC VERTEBRA AND DISC MODELS FROM SEGMENTATION WITH SELECTIVE SMOOTHING

Kati Nispel[1,2], Ann-Marie Scherzberger[2], Tanja Lerchl[1], Gabriel Gruber[1], Hendrik Moeller[1], Robert Graf[1], Veit Senner[2] and Jan S. Kirschke[1]

[1] Department of Diagnostic and Interventional Neuroradiology, School of Medicine and Health, Klinikum rechts der Isar, Technical University of Munich
Ismaninger Str. 22, 81675 Munich, Germany
kati.nispel@tum.de

[2] Associate Professorship of Sport Equipment and Sport Materials, School of Engineering and Design, Technical University of Munich
Boltzmannstr. 15, 85748 Munich, Germany

Key words: Smoothing, Intervertebral Disc, Vertebra, Triangulated Mesh, FEM.

Abstract. Due to limited MRI resolution, patient-specific simulation models derived from medical images often lack bio-fidelity. To address this, we present a smoothing pipeline for generating high-fidelity meshes of vertebrae and intervertebral discs from medical images, which serve as a base for biomechanical simulations. Using a diverse array of vertebrae smoothing algorithms, including Laplace, HC Laplace, Taubin, and Two Step, alongside surface subdivision methods such as Tri-to-Quad by 4-8, Loop, LS3-Loop, Catmull-Clark, and Butterfly, we systematically explored 136 combinations across six protocols to determine an optimal smoothing pipeline. Subsequently, an adaptive smoothing algorithm was developed for intervertebral disc meshes. By adjusting intervertebral disc vertex locations to those of the vertebra mesh, we ensured seamless alignment of contact surfaces including shared nodes. Evaluation of our pipeline against conventional smoothing methods demonstrates superior edge preservation and reduced stair-step effects, enhancing the fidelity of the generated meshes. Finite Element Method simulations further confirmed the accuracy of our selective smoothing pipeline, showing increased notch stress. Our pipeline, validated on a diverse dataset, offers an automated solution for generating patient-specific vertebrae and intervertebral disc models with enhanced biomechanical fidelity, enabling comprehensive studies in large cohorts and deeper insights into spine biomechanics and pathology.

1 INTRODUCTION

Spinal pathologies encompass a range of conditions affecting the spine, including, e.g., low back pain, neck pain, scoliosis, spinal stenosis, and degenerative disc disease [16]. In addition, traumatic injuries such as wedge fractures of vertebrae occur with increasing degeneration [23]. These conditions have significant implications for patients' quality of life and often require long-term support and treatment, including surgery [26].

Numerous studies investigated degenerative changes in vertebrae [14, 17] and IVDs [11, 30, 33] using either multibody simulation (MBS) [26, 21] or the finite element method (FEM) [10, 28]. Significantly fewer authors have generated their models patient-specifically [8, 9, 18, 19, 30], despite considerable proof of unique model characteristics leading to more diverse results [24, 13,

20]. Most patient-specific modeling approaches apply mesh morphing methods, which are based on landmark extraction from patient-specific medical images and subsequent deformation of predefined reference mesh [8, 18, 3]. Once the target geometry gets more complex, larger deformations have to be performed during the morphing process, which can lead to decreasing mesh quality [22]. Deriving meshes directly from a medical scan using the marching cubes algorithm can be advantageous due to it recreating segmented bodies directly based on the source. However, resolutions of common MRI and CT images are limited, leading to low-resolution representations of the biological state, respectively [26]. These artifacts alter the body's geometry, which is commonly known to impact FEM results. In vertebrae, artifacts like the stair-step effects are known to significantly impact the accuracy of FEM results [2]. As these generated surface meshes serve as a baseline for later FEM model models, the implementation of mesh smoothing is inevitable for accurate biomechanical simulations.

While previous studies have addressed the need for smoothing processes [27, 2], few have provided comprehensive descriptions of the applied smoothing protocols [18, 3, 10, 28]. Commonly, low resolution-caused artifacts like stair-steps are compensated using overall vertebra smoothing [27]. This approach may result in features like vertebra edges or osteophytes being smoothed to the point of disappearance, which likely affects respective simulation results in later stages. Vertebrae are more complex in shape and thus pose a greater challenge for smoothing protocols, while IVDs seem less of a challenge. However, distinctly smoothing them would result in non-coherent contact surfaces. In turn, computational efficiency decreases, potentially leading to convergence issues and less accurate results [31, 12]. Further, the absence of coherent contact surfaces, or more specifically, shared contact nodes, can be disadvantageous for coupled MBS and FEM simulations [1].

In this context, the primary objectives of this study include achieving smooth endplate (EP) surfaces on vertebrae meshes, ensuring precise coherence with IVD surfaces, and preserving characteristic bone structures such as osteophytes and sharp edges. Additionally, we investigate an adaptive smoothing algorithm to seamlessly integrate IVD meshes into the overall spine model. By addressing these challenges, our work aims to enhance the accuracy and reliability of patient-specific biomechanical models, ultimately facilitating the translation of biomechanical simulations into routine clinical practice to offer personalized treatment options.

2 METHODS

A subset of the German National Cohort (GNC) [7] containing 31 MRI scans was used to develop and evaluate the smoothing pipeline, here referred to as the GNC dataset. Vertebrae with labels 5 - 23 and the respectively associated IVDs were segmented using the automated approach SPINEPS [25]. Since CT segmentations are more adequate in capturing characteristic bone structures that deviate from the norm (Figure 1), we used a second dataset to investigate the pipeline performance regarding stair-step smoothing and edge maintenance in those extreme cases. The dataset was a retrospective, internal dataset containing rigidly, point-registered CT and MRI images [15], and is here referred to as the internal dataset. CT segmentations were created using an automated algorithm by Sekuboyina et al. [4], and MRI segmentations again using SPINEPS [25]. The segmented IVD and EP masks were subsequently transferred to the CT image segmentation. For both datasets, segmented vertebrae and IVDs were converted to triangulated surface meshes using the marching cubes algorithm. EPs were considered part of the IVD.

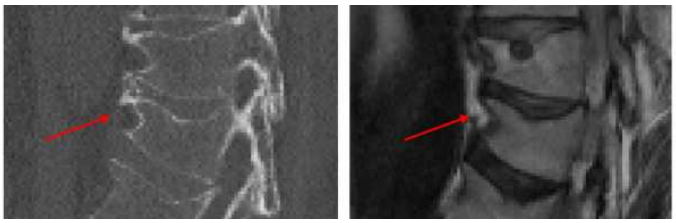

Figure 1: CT (left) vs. MRT (right) scan of the same subject. Characteristic bone structures are represented in the CT.

We first developed a smoothing pipeline for vertebra meshes and subsequently accounted for the seamless integration of the IVD meshes by implementing an adaptive smoothing algorithm. The development process was based on the GNC dataset including MRI-segmented vertebrae. The point-registered dataset served as subsequent validation data.

2.1 Vertebrae Smoothing Algorithm Development using the GNC Dataset

Using the GNC dataset, we implemented and combined a range of mesh processing methods for vertebrae. Broadly, methods can be divided into basic mesh smoothing algorithms (BSA) and surface subdivision methods (SSM). Implemented BSA included Laplace, HC Laplace, Taubin and the Two Step algorithm. As SSM, we investigated Tri-to-Quad by 4-8 subdivision, Loop, LS3-Loop, Catmull-Clark and the Butterfly approach. Besides varying these algorithms and approaches in their parameters and orders, we distinguished between applying them either to the complete meshes or to selected parts. In the latter case, we further differentiated the parameters used to select the specific parts of the mesh, namely the normal vectors of elements or the distance of nodes to the adjacent IVD mesh. All mesh processing methods are summarized in Table 1. In total, we implemented seven different protocols, each of which consisted of a different combination of the above-mentioned mesh processing methods. Figure 2 summarizes the seven approaches, divided into Approach 1, Approach 2 a), b) and c), as well as Approach 3 a), b) and c).

Table 1: All mesh processing methods tested during the development process of the vertebra smoothing algorithm.

BSA	**SSM**	**Selective**
– Laplace	– Tri-to-Quad by 4-8	– based on normal vector
– HC Laplace	– Loop	- Gaussian Filter
– Taubin	– LS3-Loop	- Bilateral Filter
– Two step	– Catmull-Clark	– based on IVD distance
	– Butterfly	

Approach 1: BSA and SSM

The first approach aimed to remove stair-steps and preserve edges by applying various combinations of BSA and SSM. In total, 136 combinations were tested, which can broadly be divided into six protocols:

- **Protocol 1:** BSA solely, with iterations from 3 to 100 and various smoothing settings. For the Taubin filter, parameters were varied between $0.3 \leq \lambda \leq 0.9$ and $\mu = -\lambda + 0.3$. For the Two Step filter, we varied angles from 5° to 80°.

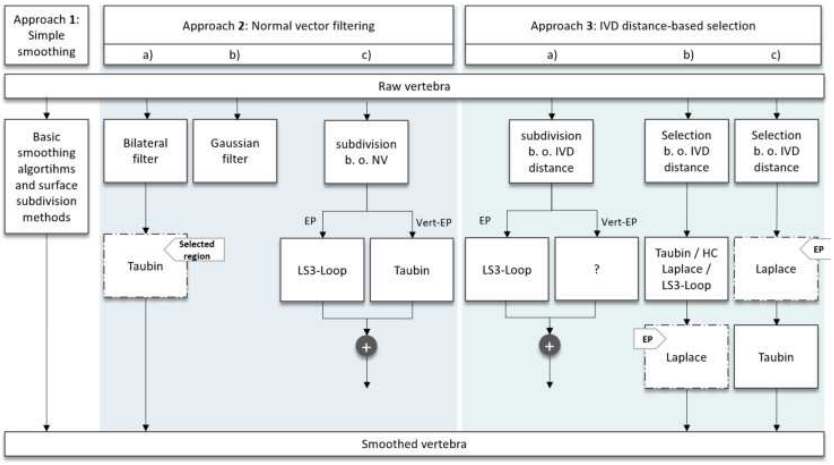

Figure 2: Note that the dashed lines indicate a selected, separate region in the mesh. Junctions indicate the creation of two distinct submeshes.

- **Protocol 2:** Combined BSA, applying one after another, totaling twelve combinations. Iterations and parameters were similar to Protocol 1.
- **Protocol 3:** Added SSM (Tri-to-Quad, Loop, LS3-Loop, Catmull-Clark, Butterfly) to the combinations in Protocol 2, resulting in 72 combinations. Iterations ranged from 1 to 30 cycles, with edge thresholds from 1-15% or 90-99%.
- **Protocol 4 and 5:** In Protocol 4, we applied the SSM directly to the output of one basic smoothing algorithm instead of using a combination of BSA as a basis. In contrast, we first applied an SSM and then a basic smoothing algorithm in Protocol 5. Iterations, λ, μ, angles, and edge thresholds were equal to Protocol 1-3.

Approach 2: Normal vector filtering

Two distinct approaches have been employed using normal vector filtering methods. In 2a), we used a bilateral filter with edge-angle thresholds from 5° to 90° and iterations from 1 to 50 cycles. The bilateral filter was applied to three coordinate directions, combined in twelve sequences. We then applied the Taubin smoothing algorithm with 30 iterations and $\lambda = 0.8$. In contrast, Approach 2b) focused on smoothing vertices based on the differences in angle between their associated normal vectors. This approach employs a Gaussian filter with a standard deviation (σ) of 1 for angle differences within a threshold range of 5° to 80°. In Approach 2c), we separated the EP from the vertebra using angle differences, smoothing them with the LS3-Loop algorithm (20 iterations, 99% edge threshold), and the remaining vertebra with the Taubin filter (15 iterations, $\lambda = 0.5$, $\mu = -\lambda + 0.3$). Note that in 2c), the mesh was split into two separate parts.

Approach 3: Selective Smoothing based on IVD distance

Three different approaches were applied that made use of the IVD meshes resulting from the segmentation mask by selecting the EP contact surfaces based on distance thresholds ranging from 0.6 to 0.8mm. In approach 3a), EP surfaces were smoothed with LS3-Loop (20 iterations, 99%

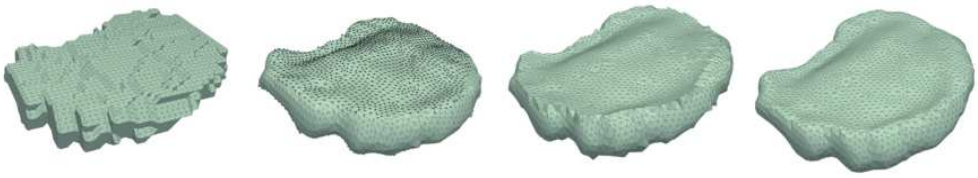

Figure 3: Exemplary smoothing process of IVD mesh. From left to right: Raw mesh, preprocessed, adaptively smoothed and postprocessed mesh.

edge threshold), and the remaining vertebra mesh with a basic smoothing algorithm. In 3b), the entire vertebra underwent Taubin smoothing (20-50 iterations, $0.5 \leq \lambda \leq 0.7$, $\mu = -\lambda + 0.03$), HC Laplace (20-50 iterations, $0.5 \leq \lambda \leq 0.9$), or LS3-Loop (5-20 iterations, edge thresholds ranging from 1°-7°and 95°-99°). EP surfaces were smoothed separately using Laplace filtering with parameters $\lambda = 0.05 - 0.3$ and 40-90 iterations. In approach 3c), the smoothing process was reversed compared to 3b). Initially, EP surfaces were smoothed using Laplace filtering with parameters $0.05 \leq \lambda \leq 0.3$ and 40-90 iterations. Subsequently, the entire vertebra underwent Taubin filtering with parameters (20-50 iterations, $0.5 \leq \lambda \leq 0.7$ and $\mu = -\lambda + 0.03$).

2.2 Adaptive IVD Smoothing

Based on the vertebrae smoothing, the adaptive IVD smoothing algorithm was implemented 3. A Taubin filter ($\lambda = 0.5, \mu = -0.53$) and 5% dilation were applied before we identified the interface vertices of the IVDs using smoothed adjacent vertebrae meshes and the previously determined distance thresholds. A nearest neighbor function was employed to identify the closest vertex on the adjacent vertebra mesh for each interface vertex in the IVD mesh. Correspondence between interface vertices was established by replacing the IVD vertex locations with those of the vertebra mesh, facilitating seamless alignment. Taubin filtering ($\lambda = 0.5, \mu = -0.53$) ensured mesh quality in a postprocessing step.

2.3 Algorithm Performance Validation

We evaluated all the resulting vertebrae smoothing algorithms based on their ability to (I) produce a smooth EP surface, (II) create a coherent contact surface between IVD and vertebra, and (III) preserve characteristic bone shapes. The bio-fidelity of the EP surfaces was evaluated by visual inspection, focusing on the absence of stair-step effects. Increased EP smoothness correlates with decreased edge sharpness for smoothing filters applied to the whole mesh, which was considered during the result evaluation. Additionally, we calculated the curvature using the quadric fitting method, which approximates mesh nodes and associated normals by a quadratic surface. The coherence of the vertebra and IVD contact surface was evaluated by the distance of their interface nodes. To evaluate edge preservation in severe cases like osteophytes or fractures, we used the point-registered dataset. Conventionally smoothed meshes were compared to selectively smoothed meshes visually. In an additional FEM simulation, notch stress was analyzed for conventional vs. selective smoothing. Therefore, linear material parameters were assumed, and a moment load was applied to the nodes that represented the IVD contact region. FEM models were generated and simulated using an automated pipeline [29].

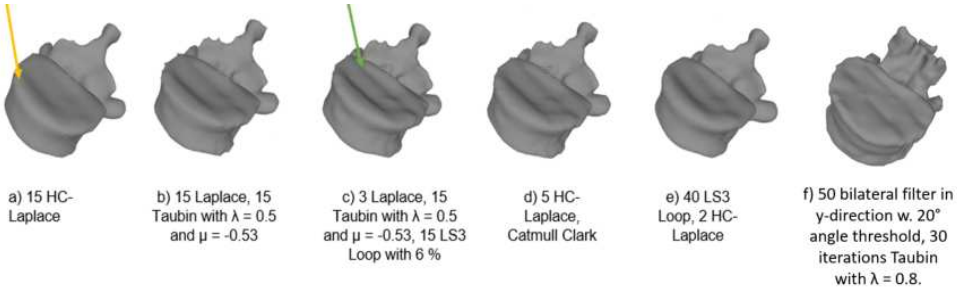

Figure 4: Example result of Approach 1 with a) BSA with a yellow arrow showing the crease edge. b) two combined BSA. c) two combines BSA with a subdivision surface method. A green arrow points at the stair-step effect. d) basic smoothing approach and surface subdivision method. e) subdivision method and a basic smoothing algorithm. f) axis-dependent, bilateral filter and subsequent Taubin algorithm.

3 RESULTS

We developed a smoothing pipeline for vertebra and IVD smoothing, which achieves smooth EP surfaces, ensuring precise coherence of vertebra and IVD surfaces while preserving characteristic bone structures such as osteophytes and sharp edges.

3.1 Smooth EP Surfaces

In the vertebra smoothing process, Approach 1 tried to smooth the whole vertebra with different combinations of BSAs and SSMs (Figure 4). We found that removing the stair-steps needed a lot of smoothing, which then over-smoothed the sides and the edges, resulting in a loss of detail (Figure 4 a)). No matter the combinations and iterations, no compromise was found in Approach 1, which retained edge details and simultaneously smoothed stair-steps (Figure 4 b-f).

Selectively smoothing a bilaterally filtered region of the vertebra (Approach 2a)) showed better results for the edge than Approach 1, but stair-steps were persisting. As the bilateral filter is based on a coordinate system, we experienced problems for varying spine curvatures or different image modalities. The Gaussian filter overcame these issues by referring to the angle difference between the normal vectors of the vertices and their neighbors. However, due to the variation of characteristics of the vertebrae, no unique angle difference for the entire spine of one patient, nor for different patients, could be found. Separating the EP contact surface from the remaining vertebra and smoothing them as separate meshes (Approach 2c) and 3a)) caused low-quality mesh regions during mesh reconnection.

Further, we used the segmented IVDs, more precisely, their resulting surface meshes, to selectively smooth the vertebra EP surfaces while.

Approaches 3b) and c) involved selecting and smoothing the EP contact surfaces separately while maintaining their connection to the vertebrae. Considering selection distance thresholds, adjustment according to cervical, thoracic, and lumbar spine was found less effective than categorizing based on vertebrae labels: labels 5-7 with a 0.6mm threshold, 8-16 with a 0.7mm threshold, and 17-23 with a 0.8mm threshold. 80 iterations were found to deliver visually good results. As the Laplace filter was able to remove the stair-step effect in Approach 1, we used 80 iterations for smoothing the EP surface. No shrinkage issues were observed as smoothing was applied to a surface only. However, it was challenging to estimate how much the vertebra still needed to be smoothed in order to sufficiently smooth but not over-smooth the parts of the EP surfaces that

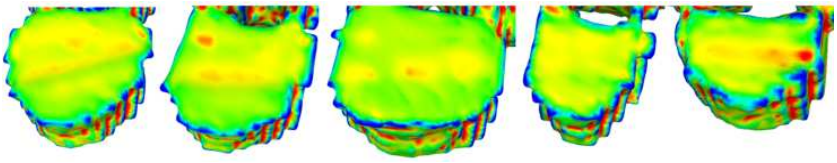

Figure 5: Mean curvature calculated with the quadric fitting method. Color mapping is based on a 10% scale. Strongest convex curvatures are indicated by the color blue, while green represents a low curvature and red the strongest concave curvature.

would not be affected by the latter selective smoothing. In Approach 3c), the entire vertebra was smoothed before selectively smoothing the EP contact surfaces. Using the Laplace filter for the entire vertebra was precluded due to the results from Approach 1. The LS3-Loop SSM, HC Laplace algorithm caused a strong volume decrease and additionally over-smoothed the edge. The Taubin filter provided better volume retention, maintained edges more appropriately, and allowed more precise adjustments without over-smoothing. Final smoothing parameters are summarized in Table 2.

Additionally, applying a curvature representation to vertebrae smoothed with the selective smoothing pipeline (Approach 3c) showed negligible signs of stair-step artifacts on the EP surface (Figure 5).

Table 2: Final parameters for the selective smoothing pipeline, including the distance thresholds for contact surface determination and EP surface smoothing parameters.

Parameter			
Distance thresholds (mm)	Labels 5-7: 0.6	Labels 8-16: 0.7	Labels 17-23: 0.8
Laplace Smoothing Parameters (EP)	Labels 5 - 15: 0.2 w. 80 iterations	Labels 16 - 21: 0.15 w. 80 iterations	Labels 22 - 23: 0.2 w. 80 iterations
Taubin Smoothing Parameters (entire vertebra)	Labels 5 - 14: $\lambda = 0.5, \mu = -0.53$, 30 iterations		Labels 15 - 23: $\lambda = 0.6, \mu = -0.63$, 30 iterations

3.2 Coherent Interface between Vertebra and IVD

Adaptive IVD smoothing was applied using the selective smoothing Approach 3c, which proved superior to other methods. The contact areas of the vertebra and IVD surfaces were well-aligned and non-intersecting, with shared node locations between the IVD and vertebrae. (Figure 6).

3.3 Edge Preservation

For more complex vertebrae from the internal dataset (CT segmented bones), the selective smoothing pipeline showed significantly better edge preservation for characteristic bone structures compared to the conventional approach, represented by 10 iterations of the HC Laplace algorithm (Figure 7). The shape of the selectively smoothed mesh closely followed the raw version, containing the fundamental bone structure. In contrast, detail was lost during the conventional smoothing approach. FEM simulation results showed an increased notch stress for the models resulting from the selective smoothing pipeline compared to a conventional one (Figure 8).

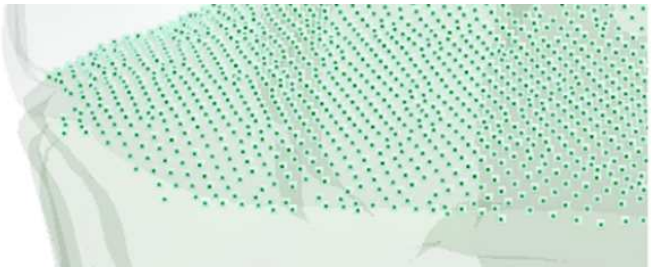

Figure 6: Shared-nodes contact surface of an exemplary vertebra and IVD. IVD nodes are colored turquoise, and vertebra nodes are represented in green.

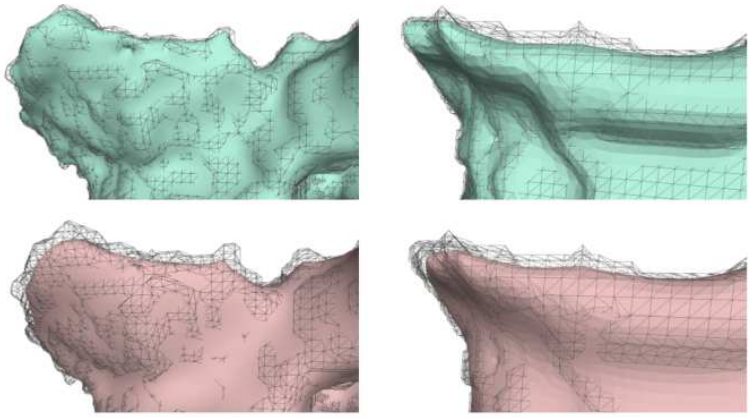

Figure 7: Comparison of selective smoothing results (top row in green) and conventional smoothing, represented by 10 iterations of HC Laplace (bottom row in red). The wireframe views display the unsmoothed version, while the face views display the differently smoothed versions.

4 DISCUSSION

The objective of this study was to develop an automated smoothing pipeline for vertebra and IVD meshes that removes resolution artifacts and maintains patient-specific details, which was achieved by using the settings of Approach 3c), here referred to as our approach or the selective smoothing pipeline.

As the developed pipeline is based on a single Python script, the process can be described as automated. In comparison with the pipeline of Caprara et al., [3], it is not necessary to further adjust the file by, for example, cropping the image.

Being able to automatically detect the biological EP contact surfaces with the help of the segmented and labeled IVD data represents a novel advancement to the best of our knowledge. In the literature, the contact region between a vertebra and an adjacent IVD is commonly assumed to contain the complete EP surface [3, 9, 18, 8]. However, IVD and vertebra contact is considered to vary in shape and size, depending on the individual anatomy and pathology. Recent segmentation algorithms represent the anatomical contact surface more appropriately by segmenting both IVDs and vertebrae [25]. Being based on these segmentations, our pipeline is the first to consider the anatomical contact surface, even upgraded by shared nodes. Besides the possibility to use this information for anatomically correct load implementation in FEM simulations, as implemented

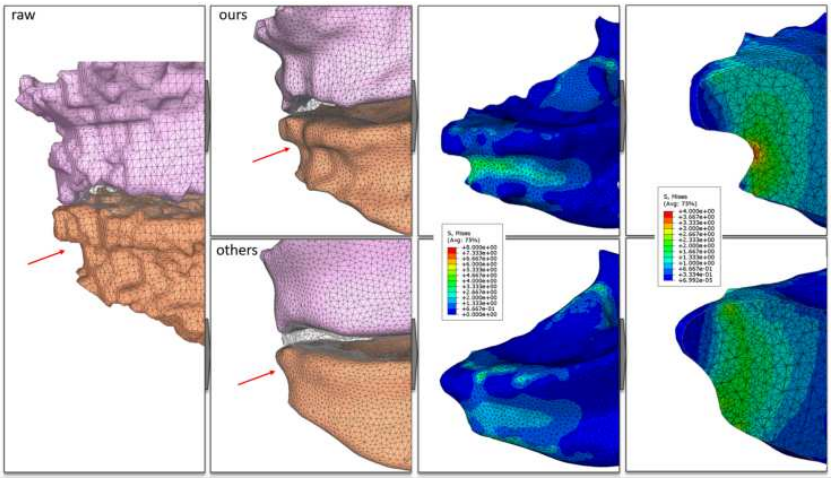

Figure 8: Notch stress in models derived from a conventional smoothing algorithm (10 iterations HC Laplace) and our selective smoothing pipeline. Starting from a raw mesh, smoothed meshes are created and converted into FEM models. A section view on the right visualizes the stress in the respective models. Note that the stress scale limit has been adapted for this view due to visualization reasons.

in our study for one exemplary vertebra, this circumstance is highly beneficial in terms of computation times. A study [12] showed that implementing shared-node contact surfaces decreased the simulation time of a comprehensive spinal model from months to only 3min. While in this study, the shared node surfaces were generated manually for a single generic spine, our smoothing approach is fully automated.

Compared to mesh morphing methods to generate vertebrae and IVD meshes [8, 18, 3, 22], the here developed, selective smoothing pipeline preserves anatomical bone structures such as osteophytes. This resulted in increased peak stress in the FEM results. Since notch stress is directly correlated with fracture risk [32], our selective smoothing pipeline could enhance the accuracy of fracture predictions in patients compared to approaches applying conventional smoothing methods.

While our pipeline produces bio-fidelic EP surfaces and preserved edges, further enhancement can be achieved by additionally smoothing the lateral surfaces of vertebrae. While the material parameters used in our FEM simulation for edge preservation were not directly related to biological conditions, future investigations could involve comprehensive FEM mesh generation integrating biological material parameters derived from bone densitometry measurements in point-registered MRI and CT datasets [14].

Further, slight vertex shifts in the IVD postprocessing cause small regions of incoherent vertebrae and IVD contact surfaces. However, the affected regions are small, and the effect on computation time remains unclear. Due to the natural limitation of digital images, an ultimate validation of the smoothing results generated by our pipeline can only be achieved by a comparsion to to cadaveric human vertebrae. However, Kanawati et al. investigated the geometric and volumetric relationship between human lumbar vertebrae and CT-based models, finding only a 1mm difference between CT models and cadaveric vertebrae [6].

5 CONCLUSION

Smoothing processes for the vertebrae and IVDs have been given little attention yet. Therefore, we created an innovative, completely automated smoothing pipeline for vertebrae and IVDs

based on segmentation data, which resolves artifacts on EP surfaces and retains characteristic bone structures of vertebrae, all while realizing a shared-node contact surface. We expect our pipeline to aid in the automation of patient-specific modeling processes while simultaneously improving the results of sole FEM simulations and co-simulations of MBS and FEM.

Acknowledgments

This research was funded by the European Research Council (ERC) under the European 530 Union's Horizon 2020 research and innovation program. Grant-Nr.: 101045128 — iBack-epic — 531 ERC-2021-COG.

REFERENCES

[1] K. Nispel, T. Lerchl, V. Senner, and J.S. Kirschke, *Recent Advances in Coupled MBS and FEM Models of the Spine-A Review*, Bioengineering (Basel), (2023).

[2] K.H. Shivanna, B.D. Adams, V.A. Magnotta, and N.M. Grosland, *Towards Automating Patient-specific Finite Element Model Development*, in *Computational Biomechanics For Medicine*, (2006), 85-93.

[3] S. Caprara, F. Carrillo, J.G. Snedeker, M. Farshad, and M. Senteler, *Automated Pipeline to Generate Anatomically Accurate Patient-Specific Biomechanical Models of Healthy and Pathological FSUs*, Frontiers in Bioengineering and Biotechnology, 9, (2021).

[4] A. Sekuboyina et al., *VerSe: A Vertebrae labelling and segmentation benchmark for multi-detector CT images*, Medical Image Analysis, 73, (2021), 102166.

[5] C. Schulz, *Approximation von Krümmungsinformation für die medizinische Visualisierung*, Diplomarbeit, Otto-von-Guericke-Universität Magdeburg, (2005).

[6] A. Kanawati, R.J.R. Fernandes, A. Gee, J. Urquhart, F. Siddiqi, and K. Gurr, *Geometric and Volumetric Relationship Between Human Lumbar Vertebra and CT-based Models*, Academic Radiology, 28, (2021), e172-e181.

[7] F. Bamberg et al., *Whole-Body MR Imaging in the German National Cohort: Rationale, Design, and Technical Background*, Radiology, 277, 1, (2015), 206-220.

[8] J.Q. Campbell and A.J. Petrella, *An Automated Method for Landmark Identification and Finite-Element Modeling of the Lumbar Spine*, IEEE Transactions on Biomedical Engineering, 62, 11, (2015), 2709-2716.

[9] I. Castro-Mateos, J. Pozo, A. Lazáry, and A. Frangi, *Automatic construction of patient-specific finite-element mesh of the spine from IVDs and vertebra segmentations*, (2016), 97881U.

[10] M. Dreischarf et al., *Comparison of eight published static finite element models of the intact lumbar spine: Predictive power of models improves when combined together*, Journal of Biomechanics, 47, 8, (2014), 1757-1766.

[11] W. Ehlers, N. Karajan, and B. Markert, *An extended biphasic model for charged hydrated tissues with application to the intervertebral disc*, Biomechanics and Modeling in Mechanobiology, 8, 3, (2009), 233-251.

[12] I. El Bojairami, K. El-Monajjed, and M. Driscoll, *Development and validation of a timely and representative finite element human spine model for biomechanical simulations*, Scientific Reports, 10, 1, (2020), 21519.

[13] M.R. Fasser, M. Jokeit, M. Kalthoff, D.A. Gomez Romero, T. Trache, J.G. Snedeker, M. Farshad, and J. Widmer, *Subject-Specific Alignment and Mass Distribution in Musculoskeletal Models of the Lumbar Spine*, Frontiers in Bioengineering and Biotechnology, 9, (2021), 721042.

[14] I. Fleps and E.F. Morgan, *A Review of CT-Based Fracture Risk Assessment with Finite Element Modeling and Machine Learning*, Current Osteoporosis Reports, 20, 5, (2022), 309-319.

[15] R. Graf, J. Schmitt, S. Schlaeger, H.K. Möller, V. Sideri-Lampretsa, A. Sekuboyina, S.M. Krieg, B. Wiestler, B. Menze, D. Rueckert, and J.S. Kirschke, *Denoising diffusion-based MRI to CT image translation enables automated spinal segmentation*, European Radiology Experimental, 7, 1, (2023), 70.

[16] P. Gruber and T. Boeni, *History of Spinal Disorders*, in *Spinal Disorders: Fundamentals of Diagnosis and Treatment*, eds. N. Boos and M. Aebi, Springer Berlin Heidelberg, (2008), 1-37.

[17] K. Imai, *Computed tomography-based finite element analysis to assess fracture risk and osteoporosis treatment*, World Journal of Experimental Medicine, 5, 3, (2015), 182-7.

[18] C.E. Lavecchia, D.M. Espino, K.M. Moerman, K.M. Tse, D. Robinson, P.V.S. Lee, and D.E.T. Shepherd, *Lumbar model generator: a tool for the automated generation of a parametric scalable model of the lumbar spine*, Journal of the Royal Society Interface, 15, 138, (2018), DOI: 10.1098/rsif.2017.0829.

[19] T. Lerchl, M. El Husseini, A. Bayat, A. Sekuboyina, L. Hermann, K. Nispel, T. Baum, M.T. Löffler, V. Senner, and J.S. Kirschke, *Validation of a Patient-Specific Musculoskeletal Model for Lumbar Load Estimation Generated by an Automated Pipeline From Whole Body CT*, Front Bioeng Biotechnol, 10, (2022), 862804.

[20] T. Lerchl, K. Nispel, T. Baum, J. Bodden, V. Senner, and J.S. Kirschke, *Multibody Models of the Thoracolumbar Spine: A Review on Applications, Limitations, and Challenges*, Bioengineering (Basel), 10, 2, (2023), DOI: 10.3390/bioengineering10020202.

[21] T. Lerchl, K. Nispel, J. Bodden, A. Sekuboyina, M. El Husseini, C. Fritzsche, V. Senner, and J.S. Kirschke, *Musculoskeletal spine modeling in large patient cohorts: How morphological individualization affects lumbar load estimation*, Front Bioeng Biotechnol, (2024).

[22] A. Malandrino, J.M. Pozo, I. Castro-Mateos, A.F. Frangi, M.M. van Rijsbergen, K. Ito, H.J. Wilke, T.T. Dao, Mchb Tho, and J. Noailly, *On the relative relevance of subject-specific*

geometries and degeneration-specific mechanical properties for the study of cell death in human intervertebral disk models, Frontiers in Bioengineering and Biotechnology, 3, (2015), DOI: 10.3389/fbioe.2015.00005.

[23] L.J. Melton III, S.H. Kan, M.A. Frye, H.W. Wahner, W.M. O'Fallon, and B.L. Riggs, *Epidemiology of vertebral fractures in women*, American Journal of Epidemiology, 129, 5, (1989), 1000-1011.

[24] L. Meszaros-Beller, M. Hammer, J.M. Riede, P. Pivonka, J.P. Little, and S. Schmitt, *Effects of geometric individualisation of a human spine model on load sharing: neuro-musculoskeletal simulation reveals significant differences in ligament and muscle contribution*, Biomechanics and Modeling in Mechanobiology, (2023), DOI: 10.1007/s10237-022-01673-3.

[25] H. Moeller et al. *SPINEPS - Automatic Whole Spine Segmentation of T2-weighted MR images using a Two-Phase Approach to Multi-class Semantic and Instance Segmentation*, European Radiology (submitted), (2024).

[26] L. Molinari and C. Falcinelli, *On the human vertebra computational modeling: a literature review*, Meccanica, 57, (2021), DOI: 10.1007/s11012-021-01452-x.

[27] T. Mönch, S. Adler, and B. Preim, *Staircase-Aware Smoothing of Medical Surface Meshes*, Proceedings of the Eurographics Workshop on Visual Computing for Biomedicine (VCBM), (2010), 83-90.

[28] S. Naoum, A.V. Vasiliadis, C. Koutserimpas, N. Mylonakis, M. Kotsapas and K. Katakalos, *Finite Element Method for the Evaluation of the Human Spine: A Literature Overview*, Journal of Functional Biomaterials, 12, 3, (2021), DOI: 10.3390/jfb12030043.

[29] K. Nispel, T. Lerchl, G. Gruber, H. Moeller, R. Graf, V. Senner and J. S. Kirschke, *From MRI to FEM: An automated pipeline for biomechanical simulations of vertebrae and intervertebral discs [in preparation], Frontiers in Bioengineering and Biotechnology (2024)*

[30] S. Natarajan, A. Tiulpin, L. Humbert, and M.A.G. Ballester, *MRI2Mesh: Intervertebral Disc Mesh Generation from Low Resolution MRI Using Graph Neural Networks with Cross Level Feature Fusion*, 2023 IEEE 20th International Symposium on Biomedical Imaging (ISBI), (2023), DOI: 10.1109/ISBI53787.2023.10230651.

[31] P. Papadopoulos and R.L. Taylor, *A mixed formulation for the finite element solution of contact problems*, Computer Methods in Applied Mechanics and Engineering, 94, 3, (1992), 373-389.

[32] G. Pluvinage, *On notch fracture mechanics*, Industrial laboratory. Diagnostics of materials, 87, (2021), 56-64.

[33] M.A. Stadelmann, G. Maquer, B. Voumard, A. Grant, D.B. Hackney, P. Vermathen, R.N. Alkalay, and P.K. Zysset, *Integrating MRI-based geometry, composition and fiber architecture in a finite element model of the human intervertebral disc*, Journal of the Mechanical Behavior of Biomedical Materials, 85, (2018), 37-42.